Ⓔ

THE ALL-WAVELENGTH EXTENDED GROTH STRIP INTERNATIONAL SURVEY (AEGIS) DATA SETS

M. DAVIS,[1] P. GUHATHAKURTA,[2] N. P. KONIDARIS,[2] J. A. NEWMAN,[3,4] M. L. N. ASHBY,[5] A. D. BIGGS,[6] P. BARMBY,[5]
K. BUNDY,[7] S. C. CHAPMAN,[7] A. L. COIL,[3,8] C. J. CONSELICE,[9] M. C. COOPER,[1] D. J. CROTON,[1] P. R. M. EISENHARDT,[10]
R. S. ELLIS,[7] S. M. FABER,[2] T. FANG,[1] G. G. FAZIO,[5] A. GEORGAKAKIS,[11] B. F. GERKE,[12] W. M. GOSS,[13] S. GWYN,[14]
J. HARKER,[2] A. M. HOPKINS,[15] J.-S. HUANG,[5] R. J. IVISON,[6] S. A. KASSIN,[2] E. N. KIRBY,[2] A. M. KOEKEMOER,[16] D. C. KOO,[2]
E. S. LAIRD,[2] E. LE FLOC'H,[8] L. LIN,[2,17] J. M. LOTZ,[18,19] P. J. MARSHALL,[20] D. C. MARTIN,[21] A. J. METEVIER,[2]
L. A. MOUSTAKAS,[10] K. NANDRA,[11] K. G. NOESKE,[2] C. PAPOVICH,[8,22] A. C. PHILLIPS,[2] R. M. RICH,[23] G. H. RIEKE,[8]
D. RIGOPOULOU,[24] S. SALIM,[23] D. SCHIMINOVICH,[25] L. SIMARD,[26] I. SMAIL,[27] T. A. SMALL,[21] B. J. WEINER,[8]
C. N. A. WILLMER,[8] S. P. WILLNER,[5] G. WILSON,[28] E. L. WRIGHT,[23] AND R. YAN[1]

ABSTRACT

In this the first of a series of Letters, we present a panchromatic data set in the Extended Groth Strip region of the sky. Our survey, the All-Wavelength Extended Groth Strip International Survey (AEGIS), aims to study the physical properties and evolutionary processes of galaxies at $z \sim 1$. It includes the following deep, wide-field imaging data sets: *Chandra*/ACIS X-ray, *GALEX* ultraviolet, CFHT/MegaCam Legacy Survey optical, CFHT/CFH12K optical, *Hubble Space Telescope*/ACS optical and NICMOS near-infrared, Palomar/WIRC near-infrared, *Spitzer*/IRAC mid-infrared, *Spitzer*/MIPS far-infrared, and VLA radio continuum. In addition, this region of the sky has been targeted for extensive spectroscopy using the Deep Imaging Multi-Object Spectrograph (DEIMOS) on the Keck II 10 m telescope. Our survey is compared to other large multiwavelength surveys in terms of depth and sky coverage.

Subject headings: galaxies: photometry — infrared: galaxies — radio continuum: galaxies — surveys — ultraviolet: galaxies — X-rays: galaxies

Online material: color figure

1. INTRODUCTION

The All-Wavelength Extended Groth Strip International Survey (AEGIS) is a collaborative effort to obtain deep imaging covering all major wave bands from X-ray to radio and optical spectroscopy over a large area of sky (0.5–1 deg²) with the aim of studying the panchromatic properties of galaxies over the last half of the Hubble time. The region studied, the Extended Groth Strip (EGS: $\alpha = 14^{h}17^{m}$, $\delta = +52°30'$) is an extension of and owes its name to a *Hubble Space Telescope* (*HST*) survey consisting of 28 Wide-Field Planetary Camera 2 (WFPC2) pointings carried out in 1994 by the WFPC team (Rhodes et al. 2000). This field benefits from low extinction, low Galactic/zodiacal infrared emission, and good schedulability by space-based observatories, and it has therefore attracted deep observations at essentially every accessible wavelength over this wide field.

Among deep multiwavelength fields, the EGS field provides a unique combination of area and depth at almost every wave band observable. It is 2× (for *HST*) to 4× (for *Spitzer* and *Chandra*) larger than the combined GOODS fields (Giavalisco et al. 2004), yet it has a similar range of wavelength coverage, making it ideal for studying rare classes of objects that may be absent in smaller fields. The GEMS field (Rix et al. 2004) covers a similar area to similar depths but was studied by the COMBO-17 photometric redshift survey rather than a spectroscopic survey. Most AEGIS data sets cover ~0.5–1 deg², smaller than the 2 deg² COSMOS field (Koekemoer & Scoville 2005). However, AEGIS observations are deeper at most wavelengths, benefiting from easier schedulability and lower foreground emission. Spectroscopy of the COSMOS field is in progress (Lilly et al. 2005) but will not be completed for 3–5 years. An additional advantage of AEGIS is that deep *HST*/ACS imaging is available in two

[1] Department of Astronomy, University of California, Berkeley, CA 94720; mdavis@berkeley.edu.
[2] UCO/Lick Observatory, University of California, Santa Cruz, CA 95064; raja@ucolick.org.
[3] Hubble Fellow.
[4] Institute for Nuclear and Particle Astrophysics, Lawrence Berkeley National Laboratory, Berkeley, CA 94720.
[5] Harvard-Smithsonian Center for Astrophysics, Cambridge, MA 02138.
[6] United Kingdom Astronomy Technology Centre, Royal Observatory, Edinburgh EH9 3HJ, UK.
[7] Department of Astronomy, California Institute of Technology, Pasadena, CA 91125.
[8] Steward Observatory, University of Arizona, Tucson, AZ 85721.
[9] School of Physics and Astronomy, University of Nottingham, Nottingham NG9 2RD, UK.
[10] Jet Propulsion Laboratory, California Institute of Technology, Pasadena, CA 91109.
[11] Imperial College London, London SW7 2BZ, UK.
[12] Department of Physics, University of California, Berkeley, CA 94720.
[13] National Radio Astronomy Observatory, Socorro, NM 87801.
[14] Department of Physics and Astronomy, University of Victoria, Victoria, BC V8W 3P6, Canada.

[15] School of Physics, University of Sydney, NSW 2006, Australia.
[16] Space Telescope Science Institute, Baltimore, MD 21218.
[17] Department of Physics, National Taiwan University, Taipei 106, Taiwan.
[18] Leo Goldberg Fellow.
[19] National Optical Astronomical Observatory, Tucson, AZ 85719.
[20] Kavli Institute for Particle Astrophysics and Cosmology, Menlo Park, CA 94025.
[21] Space Astrophysics, California Institute of Technology, Pasadena, CA 91125.
[22] Spitzer Fellow.
[23] Department of Physics and Astronomy, University of California, Los Angeles, CA 90095.
[24] Department of Astrophysics, Oxford University, Oxford OX1 3RH, UK.
[25] Department of Astronomy, Columbia University, New York, NY 10027.
[26] Associaton of Canadian Universities for Research in Astronomy, Herzberg Institute of Astrophysics, National Research Council, Victoria, BC V9E 2E7, Canada.
[27] Institute for Computational Cosmology, Durham University, Durham DH1 3LE, UK.
[28] *Spitzer* Science Center, California Institute of Technology, Pasadena, CA 91125.
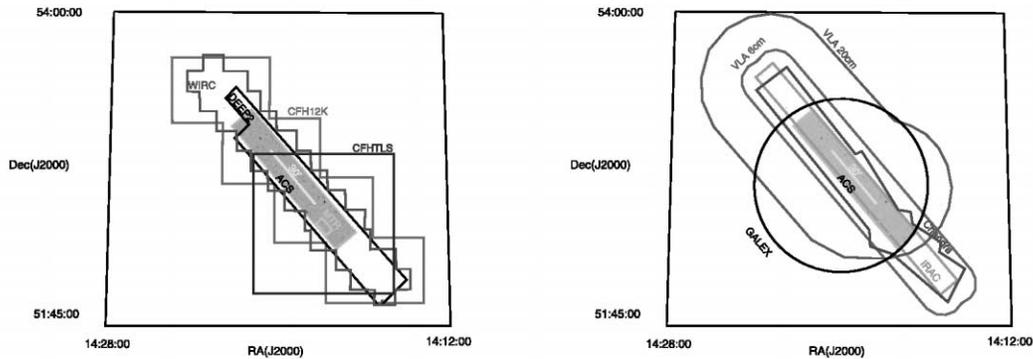
Fig. 1.—Sky coverage maps showing the AEGIS data sets. The negative gray-scale image shows the *HST*/ACS mosaic image. The outlines represent the following: *Left*: CFHT Legacy Survey MegaCam deep optical, CFHT CFH12K optical, Keck DEIMOS spectroscopy as part of the DEEP2 survey, and Palomar/ WIRC near-IR. *Right*: *Chandra*/ACIS X-ray, *GALEX* far- and near-UV, *Spitzer*/IRAC mid-IR and MIPS far-IR, and VLA radio continuum 6 cm and 20 cm. The DEEP2 outline represents the *current* spectroscopic coverage with DEIMOS; the length of the *completed* DEEP2 strip will be 2° by extending it to the northeast. The length of the *HST*/ACS mosaic is about 1°. The minitest region (MTR), shown as a small rectangle superposed on the *HST*/ACS image, is used to showcase the panchromatic SEDs of galaxies (Konidaris et al. 2007). The length of the line segment superposed on the ACS image running along its length is 30′. [*See the electronic edition of the Journal for a color version of this figure.*]

bands (F606W+F814W), in contrast to only F814W for the COSMOS field; the GEMS F850LP imaging is too shallow to study subcomponent colors for most galaxies.

Long before AEGIS, the EGS field attracted a rich suite of surveys, including spectroscopy (Lilly et al. 1995; Steidel et al. 2003; Cristóbal-Hornillos et al. 2003) and panchromatic imaging from the ground and space, including X-ray (Miyaji et al. 2004; Nandra et al. 2005), ultraviolet (UV) and optical (Beck-Winchatz & Anderson 1999; Brunner et al. 1999; Sarajedini et al. 2006), near-infrared (IR) (Cardiel et al. 2003; Hopkins et al. 2000), mid-IR (Flores et al. 1999), submillimeter (Coppin et al. 2005), and radio (Fomalont et al. 1991). AEGIS has carried this work even further; e.g., the first generation of the DEEP Galaxy Redshift Survey, DEEP1, published 620 galaxy redshifts in the WFPC2 Groth Strip region (Simard et al. 2002; Vogt et al. 2005; Weiner et al. 2005). In comparison, the successor DEEP2 Galaxy Redshift Survey has obtained 9501 redshifts in the EGS so far, with thousands more planned.

Data from DEEP2 are a linchpin for almost all AEGIS studies, providing redshifts; internal kinematics for dynamical masses; line strengths for star formation rates, AGN identification, and gas-phase metallicities; stellar population ages and metallicities; etc. The precision and relatively dense sampling of DEEP2 redshifts allow for accurate measurement of the local environment of objects in the EGS, which is a major factor driving galaxy evolution. Other surveys at similar redshifts provide weaker environmental measures due to larger redshift errors, lower sampling rates, and/or smaller areas (Cooper et al. 2005). Furthermore, we can remove cosmic variance fluctuations from observed AEGIS abundances by comparing redshift distributions to the other three, widely separated DEEP2 fields.

Ten instrument teams and a number of theorists are collaborating on AEGIS—nearly 100 scientists in half a dozen countries. The first fruits of this collaboration are presented in this issue of *Astrophysical Journal Letters*. These papers make use of the power of the combined AEGIS data set in a variety of ways. Five Letters investigate the nature of rare objects found in this field, illustrating the benefits of wide areal coverage (Huang et al. 2007; Moustakas et al. 2007; Symeonidis et al. 2007; Gerke et al. 2007; Le Floc'h et al. 2007). These studies take advantage of the full multiwavelength coverage, which provides each object's spectral energy distribution (SED) in

detail; we also explore the range of SEDs of a wider set of galaxies in Konidaris et al. (2007).

Five more Letters investigate the drivers and evolution of star formation in galaxies using the array of indicators available from this multifaceted data set: UV, IR, and radio continuum and optical emission lines (Ivison et al. 2007; Lin et al. 2007; Noeske et al. 2007a, 2007b; Weiner et al. 2007). Three Letters focus on the optical properties of active galactic nuclei (AGNs) at $z \sim 1.4$ identified using deep X-ray and IR data, and explore their relationship to their large-scale structure environment (Georgakakis et al. 2007; Nandra et al. 2007; Pierce et al. 2007). Two Letters test for evolution in the relationships between mass measures to $z \sim 1$: stellar mass versus gas kinematics in galaxies (Kassin et al. 2007) and X-ray gas emission versus galaxy kinematics in groups of galaxies (Fang et al. 2007). The remaining two Letters use DEEP2 spectroscopy to study objects that are extremely red in optical-IR color, finding that a substantial fraction of the population lies at $z < 1.4$ (Conselice et al. 2007; Wilson et al. 2007).

These papers present only the first results from AEGIS; we are just beginning to reach the potential of this many faceted data set. This Letter gives details on the AEGIS data that have been obtained so far; we only describe those survey data sets in the EGS field that are used in this special issue here. Large portions of this data set, including the DEEP2 spectra and *HST*/ ACS imaging, will be publicly released in 2007, making it a legacy for the entire community.

2. THE PANCHROMATIC DATA SETS

The sky coverage of the AEGIS multiwavelength data sets is shown in Figure 1. The acquisition and reduction of these data sets have been/will be described in separate papers. Our aim here is to summarize this information and discuss the derivation of source photometry catalogs (from which panchromatic SEDs are measured) so that the other Letters in this issue will be meaningful to readers. Table 1 contains all the basic information, and we will not repeat this in the text. *Spitzer* IRS mid-IR spectra exist for a relatively small number of galaxies; the details of these observations are in Le Floc'h et al. (2007) and Huang et al. (2007).

TABLE 1
AEGIS Data Sets

Telescope/Instr. (Mode)	Band	PSF (FWHM)	λ_{eff}	Lim. Mag. (5 σ in most cases)	Surf. Dens. (deg^{-2})	Area (deg^2)	Exp. Time (ks)
Chandra/ACIS	HB	0.5″–6.0″	3.1 Å (4 keV)	8.2×10^{-16} ergs s^{-1} cm^{-2}	3200	0.67	200
	SB	0.5″–4.0″	12.4 Å (1 keV)	1.1×10^{-16} ergs s^{-1} cm^{-2}	2500	0.67	200
GALEX	FUV	5.5″	1539 Å	25 (AB) [3 σ]	8720	1.13	58
	NUV	5.5″	2316 Å	25 (AB) [3 σ]	2.35×10^4	1.13	120
CFHT/MegaCam	u^*	<1.1″	3700 Å	26.3 (AB)	$\approx 10^5$	1	15
(CFHTLS/*current*)	g'	<1.0″	4850 Å	27.0 (AB)	$\approx 10^5$	1	35
	r'	<0.9″	6250 Å	26.5 (AB)	$\approx 10^5$	1	78
	i'	<0.9″	7700 Å	26.0 (AB)	$\approx 10^5$	1	158
	z'	<0.9″	8850 Å	25.0 (AB)	$\approx 10^5$	1	86
CFHT/CFH12K	B	1″	4389 Å	24.5 (AB) [8 σ]	1.45×10^5	1.31	6.5
	R	1″	6601 Å	24.2 (AB) [8 σ]	1.45×10^5	1.31	3.6
	I	1″	8133 Å	23.5 (AB) [8 σ]	1.45×10^5	1.31	4.7
HST/ACS	F606W (V)	0.1″	5913 Å	28.75 (AB) [5 σ]	4.0×10^5	0.197	2.3
(WFC)	F814W (I)	0.1″	8330 Å	28.10 (AB)	3.9×10^5	0.197	2.1
HST/NICMOS	F110W (J)	0.35″	1.10 μm	25.7 (AB) [10 σ]	3.3×10^5	0.0128	2.6
(NIC3)	F160W (H)	0.35″	1.59 μm	25.5 (AB) [10 σ]	3.3×10^5	0.0128	2.6
Palomar/WIRC	J	1″	1.25 μm	23 (Vega)	7.64×10^4	0.2	4–7
	K_s	1″	2.14 μm	20.6 (Vega)	5.37×10^4	0.7	4–7
Spitzer/IRAC	Band 1	1.8″	3.6 μm	0.9 μJy	1.66×10^5	0.33	10.1
	Band 2	2.0″	4.5 μm	0.9 μJy	1.68×10^5	0.33	10.1
	Band 3	2.2″	5.8 μm	6.3 μJy	4.90×10^4	0.33	10.1
	Band 4	2.2″	8.0 μm	5.8 μJy	4.86×10^4	0.33	10.1
Spitzer/MIPS	24 μm	5.9″	23.7 μm	77 μJy	1.76×10^4	0.534	1.68
	70 μm	19″	71.4 μm	10.3 mJy	1275	0.498	0.84
VLA	6 cm	1.2″	6 cm	0.6 mJy beam^{-1} [10 σ]	88.9	0.57	0.9
	20 cm	4.2″	20 cm	100 μJy beam^{-1}	1075	0.64	400

Telescope/Instr. (Mode)	Wavelen. Range (Å)	Spec. Res. (Å)	Spatial PSF (FWHM)	Lim. Mag.	Area (deg^2)	Num. Targ.	Exp. Time (ks)
Keck/DEIMOS .... (DEEP2/Spectra)	6400–9100	1.4	0.6″–1″	$R_{AB} = 24.1$	0.5 (*final*)	17,600 (*final*)	3.6

2.1. *Chandra/ACIS X-Ray Images*

The EGS region has been surveyed at X-ray wavelengths by *Chandra* using the Advanced CCD Imaging Spectrometer (ACIS).[29] At the time of writing, these observations represent the third deepest X-ray survey in the sky. The Hubble Deep Field–North survey is ~5 × deeper over a ~5 × smaller area (Alexander et al. 2003). The Chandra Deep Field–South (Giaconni et al. 2002; Lehmer et al. 2005) covers about half the AEGIS area mostly to a similar depth, with a smaller central region that is twice as deep. The vast majority of X-ray sources detected in the EGS field are AGNs. At the target redshift of the DEEP2 survey, $z = 1$, the AEGIS limiting luminosity of 7×10^{41} ergs s^{-1} corresponds to ~$0.005L_*$, where L_* is the characteristic AGN luminosity at this redshift (Barger et al. 2005).

The AEGIS *Chandra* observations consist of eight individual pointings obtained with the ACIS-I instrument, each with a field of view of $\approx 17' \times 17'$. The data reduction is performed using the CIAO data analysis software version 3.2. After rejection of artifacts and gain and charge transfer inefficiency corrections, the individual observations of a given *Chandra* pointing are merged into a single event file. The final mosaic images are used to detect sources in a number of energy bands, including 0.5–2.0, 2.0–7.0, and 0.5–7.0 keV. Candidate sources are preselected based on a low likelihood probability threshold (10^{-4}), followed by aperture count extraction using the 70% point-spread function (PSF) radius and a local background determination to estimate the source significance (for details, see

Nandra et al. 2005). The final catalog comprises sources with Poisson false probability <4×10^{-6}. Point-source fluxes are estimated by integrating the net counts within the 90% encircled energy radius at the position of the source. We adopt a power-law SED with $\Gamma = 1.4$ and Galactic neutral hydrogen column density $N_H = 1.3 \times 10^{20}$ cm^{-2}, appropriate for the EGS field. Only a subset of the AEGIS *Chandra* observations has been analyzed at this point (see Georgakakis et al. 2007).

2.2. *GALEX Ultraviolet Images*

Galaxy Evolution Explorer (*GALEX*)[30] images of the EGS were obtained in 2003, 2004, and 2005. Deep images are built from stacks of 42 far-ultraviolet (FUV) and 87 near-ultraviolet (NUV) separate one-orbit images and processed using version 4.1 of the *GALEX* pipeline.[31] The raw photon count images are flat-fielded and calibrated using relative response maps. The resulting calibrated intensity images are in units of photon s^{-1}, where 1 photon s^{-1} corresponds to 18.82 and 20.08 ABmag for the FUV and NUV bands, respectively. The background in the images is estimated using PoissonBG, a program written for *GALEX* data that uses Poisson rather than Gaussian statistics to clip suspected sources from the background map. Finally, the source catalogs are derived from the background-subtracted images using SExtractor (Bertin & Arnouts 1996).

[29] NASA's *Chandra X-Ray Observatory* was launched in 1999 July. The *Chandra* Data Archive (CDA) is part of the *Chandra* X-Ray Center (CXC), which is operated for NASA by the Smithsonian Astrophysical Observatory.

[30] *GALEX* (*Galaxy Evolution Explorer*) is a NASA Small Explorer, launched in 2003 April. We gratefully acknowledge NASA's support for construction, operation, and science analysis of the *GALEX* mission, developed in cooperation with the Centre National d'Etudes Spatiales of France and the Korean Ministry of Science and Technology.

[31] See http://www.galex.caltech.edu.

2.3. *CFHTLS/CFH12K and MegaCam Optical Images*

The EGS is one of four fields covered by the ongoing Canada-France-Hawaii Telescope Legacy Survey (CFHTLS) Deep Survey.[32] This field (labeled "D3" by CFHTLS) has been observed for a total of 114 hr using the MegaCam imager on the 4 m Canada-France-Hawaii Telescope (CFHT; Boulade et al. 2003)[33] from 2003 April to the present; a total integration time of 330 hr is planned by the end of the five year survey. This time is divided among five broadband filters: u^*, g', r', i', and z'; 5 σ point-source detection limiting AB magnitudes in the current data set range from 25.0 (in z') to 27.0 (in g').

The catalogs used in AEGIS papers are based on a subset of the CFHTLS data set with total exposure times of 1.7/1.8/4.1/13.0/1.0 hr in u^*/g'/r'/i'/z'. The data were processed through the Elixir pipeline (Magnier & Cuillandre 2004), defective exposures rejected based on visual inspection, and the astrometric and photometric calibrations improved (S. Gwyn et al. 2007, in preparation); the frames were then corrected for distortions and co-added using SWarp.[34] Photometry was then obtained using the double image mode of SExtractor (Bertin & Arnouts 1996), with i' used as reference image. The principal CFHTLS measurements used here are Kron aperture (SExtractor MAG_AUTO) AB magnitudes. In addition, photometric redshifts for CFHTLS sources were determined using photometry within matched, 1″ radius apertures (S. Gwyn et al., in preparation).[35]

The EGS was imaged in B, R, and I bands, using four overlapping pointings of the CFH12K mosaic camera (Cuillandre et al. 2001) on CFHT, as one of the four fields in the DEEP2 survey. The construction of the astrometric/photometric catalog is described by Coil et al. (2004).[36] The R-band magnitudes were measured within circular apertures of radius $3r_g$, where r_g is the σ of a Gaussian fit to the image profile; for objects where $3r_g < 1$, a 1″ radius aperture was used instead. The $B - R$ and $R - I$ colors of each object were measured using a 1″ radius aperture. The resulting BRI photometry was calibrated to the AB system within the native CFHT12K passbands (which differ significantly from the Kron-Cousins system, particularly in I) using stars observed by the Sloan Digital Sky Survey (SDSS; York et al. 2000); the BRI stellar locus is used to ensure consistency of the color system between CFH12K pointings.

2.4. *HST/ACS Optical Images*

Deep *HST* images[37] of the EGS were obtained with the Advanced Camera for Surveys (ACS) as part of GO program 10134 (PI: M. Davis). The EGS was imaged in the V (F606W) and I (F814W) bands during the period 2004 June to 2005 March using a mosaic pattern of $21 \times 3 = 63$ contiguous "tiles," an

effective area of $\sim 10.1' \times 70.5' = 710.9$ arcmin^2 following the IRAC imaging strip (§ 2.8). Tiles were observed at a position angle of 130°, or rotated by multiples of 90° relative to this value to meet guide star constraints. Each tile was observed in a four-pointing dither pattern in each filter, in order to achieve half-pixel dithering at the center of the ACS WFC, bridge the detector gap, and improve tile overlap. The final mosaic is gap-free, and each pixel is observed at least three times. Dithered pointings were combined with the STSDAS MultiDrizzle package using a square kernel. The 5 σ limiting magnitudes for a point source are $V_{F606W} = 28.14$ (AB) and $I_{F814W} = 27.52$ (AB) within a circular aperture of radius 0.12″ ($\sim$50 pixel area). For an extended object, the 5 σ limiting magnitudes are $V_{F606W} = 26.23$ (AB) and $I_{F814W} = 25.61$ (AB) for a circular aperture of radius 0.3″ ($\sim$314 pixel area).

We detected objects in summed ACS $V + I$ images and constructed initial galaxy segmentation maps using the SExtractor galaxy photometry software (Bertin & Arnouts 1996) and a detection threshold of 1.5 σ and 50 pixels. These detection maps and the ACS zero points (Sirianni et al. 2005) were applied to each band separately to create the ACS photometric catalogs.

2.5. *Keck/DEIMOS Optical Spectra*

The EGS is one of the four fields observed by the DEEP2 collaboration (Davis et al. 2003). Here we briefly describe the DEEP2 data in the EGS; for more details see Davis et al. (2005) for mask-making algorithms, S. M. Faber et al. (2007, in preparation) for full survey details, and M. C. Cooper et al. (2007, in preparation) for data reduction pipelines. Targets were selected for DEEP2 spectroscopy from the CFHT12K BRI imaging described in § 2.3. Eligible DEEP2 targets have $18.5 \leq R \leq 24.1$, >20% probability of being a galaxy (based on angular size, $B - R/R - I$ colors, and R magnitude), and surface brightness brighter than $\mu_R = R + 2.5 \log A \leq 26.5$, where A is the area of the aperture used to measure the CFHT12K R magnitude (§ 2.3); all magnitudes are AB. Each object is given a weight based on its probability of being a galaxy, its R magnitude, and whether or not it meets the DEEP2 color cut used to eliminate low-z objects in other fields [galaxies with $(B - R) < 2.45(R - I) - 0.5$, $(R - I) > 1.1$, or $(B - R) < 0.5$ all pass this cut]. This weight is used when randomly selecting among multiple objects that cannot be observed simultaneously due to DEIMOS slit-mask constraints (Davis et al. 2005). Fainter objects (particularly those with $R > 21.5$ and expected $z < 0.75$ from the color cut) are given lower weight in order to sample a range of luminosities and roughly equal numbers of galaxies below and above $z = 0.75$ (S. M. Faber et al. 2007, in preparation). Selection probabilities for each potential target are known to <1%; the median is >70% for objects with $z < 0.1$, falls to 54% at $z = 0.5$–0.6, and is flat at 73% for $z > 0.8$.

All spectra were taken with the Deep Imaging Multi-Object Spectrograph (DEIMOS; Faber et al. 2003) at the Keck II telescope using the 1200 line mm^{-1} grating.[38] Each observation uses a unique aluminum mask milled with $\sim$150 1″-wide and >3″-long slitlets over a $16' \times 4'$ area, which is observed for a minimum of 1 hr (until a target signal-to-noise ratio is reached) divided among three or more subexposures. Slitlets are tilted up to 30° to follow the photometric major axes of extended targets.

The DEEP2 spectra were reduced with an IDL pipeline heavily modified from the IDLSPEC2D package designed for SDSS (S. Burles & D. Schlegel 2007, in preparation). Spectra were extracted using both boxcar and optimized Gaussian weighting. The pipeline determines a set of candidate redshifts for each object by fitting a linear combination of templates at each possible z and finding local minima in $\chi^2(z)$; these redshifts are then evaluated and selected among by DEEP2 team members using a graphical interface. Two significant features must match the templates for a secure redshift (quality $z_q = 3$ or 4); a resolved [O II] λ3727 doublet is counted as two features.

Based on both repeated observations and tests with multiwavelength photometry, we estimate that $\lesssim$5% of $z_q = 3$ redshifts (obtained for 11% of EGS targets) are incorrect, while $\lesssim$0.5% of highest confidence, $z_q = 4$ redshifts (60% of EGS targets) are incorrect. Lower quality redshifts are considered insecure or ambiguous and are not used for any analyses. Objects with repeated observations (310 out of the 13,570 galaxies observed so far in the EGS) have an rms redshift uncertainty of 30 km s^{-1}. Secure redshifts have been obtained for 9501 galaxies in the EGS, with median redshift 0.74. Objects at $z > 1.42$ tend not to have strong features in the DEEP2 spectral window; such objects appear to comprise the bulk of DEEP2 redshift failures (C. Steidel 2006, private communication).

2.6. HST/NICMOS Near-Infrared Images

Deep HST Near-Infrared Camera and Multi-Object Spectrometer (NICMOS) NIC3 images of the EGS were obtained as "parallels" of the ACS images (§ 2.4) as part of GO program 10134 (PI: M. Davis). Each NIC3 field was observed in the J (F110W) and H (F160W) bands. A total of 63 NIC3 fields were observed, each covering $51.2'' \times 51.2''$. Of these, 58 fields fully overlap with the ACS imaging mosaic; the remaining five NIC3 pointings coincide with other AEGIS data sets. Since the NIC3 PSF is undersampled, we developed a four-point dither pattern that simultaneously provides optimal subpixel dithering for ACS WFC and NIC3 to improve the final resolution of the reduced images.

The NICMOS NIC3 images were processed in a similar way as the ACS images. Basic image reductions were performed with the `stsdas.calnica` routine: flat-fielding and corrections for dark current, bias, variable quadrant bias, amplifier glow, cosmic-ray persistence, detector nonlinearity, pixel defects, bad imaging regions, cosmic rays of unusual size, and the count rate–dependent nonlinearity. The four pointings per tile per filter were combined with the STSDAS MultiDrizzle package using a square kernel. Sources were detected using summed NIC3 $J + H$ images using SExtractor (Bertin & Arnouts 1996), using a detection threshold of 1 σ and minimum size of 10 pixels. Photometry was performed on the individual images using circular apertures of diameter $0.52''$ calibrated using the zero points in the NICMOS Data Handbook.

2.7. Palomar/WIRC Near-Infrared Images

Near-IR observations of the EGS in the J and K bands were obtained using the Wide-Field Infrared Camera (WIRC) on the Palomar 5 m telescope.[39] The observations were carried out between 2003 and 2005. WIRC has an effective field of view

of $8.1' \times 8.1'$, with a scale of $0.25''$ pixel^{-1}. The EGS observations consist of 33 WIRC overlapping pointings in K and 10 pointings in J, each with 4×30 s exposures dithered over a nonrepeating $7''$ pattern. Typical total exposure times per band at any given location within the EGS are 1–2 hr. Photometric calibration was carried out by referencing standard stars during photometric conditions. The final images were made by combining individual mosaics obtained over several nights. The images were processed using a double-pass reduction pipeline developed specifically for WIRC.

2.8. Spitzer/IRAC Mid-Infrared Images

The Spitzer mid-IR observations were carried out as part of Guaranteed Time Observvation (GTO) program 8, using time contributed by G. Fazio, G. Rieke, and E. Wright. The Infrared Array Camera (IRAC; Fazio et al. 2004) images were obtained in 2003 December and 2004 June/July.[40] Each IRAC exposure covered a $5.12' \times 5.12'$ field of view. At each of the 52 positions in a $2° \times 10'$ map, there were 52 dithered 200 s exposures at 3.6, 4.5, and 5.8 μm, together with 208 dithered 50 s exposures taken concurrently at 8.0 μm. Data processing began with the Basic Calibrated Data produced by version 11 of the Spitzer Science Center IRAC pipeline. Mosaicing was done using custom IDL scripts: the frames were distortion-corrected, registered, and averaged after rejection of artifacts (cosmic rays, scattered light, etc.). The scale of the mosaics, $0.6''$ pixel^{-1}, subsamples the native IRAC pixel scale by a factor of two. The two shorter wavelength IRAC bands are more sensitive than the longer wavelength bands.

To make catalogs, sources in the IRAC mosaics were identified using DAOPHOT/FIND and were photometered in a $3''$ diameter aperture. Aperture corrections to the IRAC calibration photometry aperture of $12.2''$ (multiplicative factors of 2.07, 2.15, 2.45, and 2.68 in the four bands) were applied. For each object, neighboring objects in a 200 pixel box were subtracted before photometry. Both 3.6 μm– and 8.0 μm–selected catalogs were generated: photometry for the objects in each was centered on the position in the mosaic in the selected band. There are about 73,000 objects in the 3.6 μm–selected catalog, many of which are undetected in the 8.0 μm mosaic; the 8.0 μm catalog contains only 16,000 objects.

2.9. Spitzer/MIPS Far-Infrared Images

Spitzer far-IR observations with the Multiband Imaging Photometer for Spitzer (MIPS; Rieke et al. 2004) were also carried out as part of the same GTO program. Data were obtained in 2004 January and June using the slow rate MIPS scan mode with legs 2.4° long. The MIPS 24 μm channel has a $5.4' \times 5.4'$ field of view (128×128 array of $2.55''$ pixels). The 70 μm channel has a $5.2' \times 5.2'$ field of view (32×32 array of $9.98''$ pixels), but only half of the array is functional. The 160 μm channel has a $5.3' \times 2.1'$ field of view (20×3 array of $16'' \times 18''$ pixels), but one row of the array is not operational. The final mosaic covers an area $\sim$2.4° $\times$ 10'. The effective integration time at 24 μm is $\sim$1500 s for locations near the long center line of the strip, decreasing to $\sim$700 s 5' from the center line. At 70 and 160 μm,

the average integration times are ∼700 and 100 s pixel^{-1}, respectively. The data were reduced and mosaicked with the MIPS Data Analysis Tool (Gordon et al. 2005). Sources were identified, and photometry extracted with PSF fitting, using the DAOPHOT software (Stetson 1987).

2.10. *VLA Radio Continuum Images*

Radio continuum observations covering a $2° × 17'$ strip at 6 cm (4.8 GHz, C band) with the VLA[41] in BnA configuration are described by Willner et al. (2006). Altogether, 51 radio components, denoted "EGS06," were detected at $≥10 \sigma$ significance. Fourteen of these components were deemed to represent seven double radio sources. More than 90% of the radio sources are identified with IRAC counterparts (Willner et al. 2006). Table 1 and Figure 1 summarize other survey properties.[42]

Observations at 20 cm (1.4 GHz, L band) with the VLA in its B configuration are described by Ivison et al. (2007). There were six pointings concentrating on the northern half of the strip (see Fig. 1). The radio images cover 0.04, 0.36, and 0.64 deg^2 to 5 σ limits of 50, 75, and 100 μJy beam^{-1}, respectively. Source detection for AEGIS20 followed that described by Biggs & Ivison (2006). The resulting catalog, AEGIS20, contains 1123 discrete radio emitters and is published in electronic form (Ivison et al. 2007).

---

[41] The Very Large Array of the National Radio Astronomy Observatory is a facility of the National Science Foundation operated under cooperative agreement by Associated Universities, Inc.

[42] Radio images available at http://www.cfa.harvard.edu/irac/publications/2006refereed/vla6cm/.

3. SUMMARY

This Letter has described the multiwavelength data set in the Extended Groth Strip assembled by the AEGIS collaboration. The remaining Letters in this special issue discuss a wide range of scientific results derived from these data. By combining deep observations at almost every wavelength available over ∼1 deg^2 of sky with the relatively high resolution spectroscopy and dense sampling of the DEEP2 Galaxy Redshift Survey, AEGIS is making possible many unique studies of the evolution of galaxies over more than half the history of the universe. The high-quality internal kinematics and environment measurements in the EGS are unmatched among deep multiwavelength fields. The data set is continuing to grow, and its potential is only beginning to be tapped; we expect AEGIS to provide a legacy long into the future.

REFERENCES

Alexander, D. M., et al. 2003, AJ, 126, 539
Barger, A. J., Cowie, L. L., Mushotzky, R. F., Yang, Y., Wang, W.-H., Steffen, A. T., & Capak, P. 2005, AJ, 129, 578
Beck-Winchatz, B., & Anderson, S. F. 1999, AJ, 117, 2582
Bertin, E., & Arnouts, S. 1996, A&AS, 117, 393
Biggs, A. D., & Ivison, R. J. 2006, MNRAS, 371, 963
Boulade, O., et al. 2003, Proc. SPIE, 4841, 72
Brunner, R. J., Connolly, A. J., & Szalay, A. S. 1999, ApJ, 516, 563
Cardiel, N., Elbaz, D., Schiavon, R. P., Willmer, C. N. A., Koo, D. C., Phillips, A. C., & Gallego, J. 2003, ApJ, 584, 76
Coil, A. L., et al. 2004, ApJ, 617, 765
Conselice, C. J., et al. 2007, ApJ, 660, L55
Cooper, M. C., et al. 2005, ApJ, 634, 833
Coppin, K., Halpern, M., Scott, D., Borys, C., & Chapman, S. 2005, MNRAS, 357, 1022
Cristóbal-Hornillos, D., Balcells, M., Prieto, M., Guzmán, R., Gallego, J., Cardiel, N., Serrano, Á., & Pelló, R. 2003, ApJ, 595, 71
Cuillandre, J.-C., Luppino, G., Starr, B., & Isani, S. 2001, in Proc. Semaine de l'Astrophysique Française, eds. F. Combes, D. Barret, & F. Thévenin (Les Ulis: EdP-Sciences), 605
Davis, M., et al. 2003, Proc. SPIE, 4834, 161
———. 2005, in ASP Conf. Ser. 339, Observing Dark Energy, ed. S. C. Wolff & T. R. Lauer (San Francisco: ASP), 128
Faber, S. M., et al. 2003, Proc. SPIE, 4841, 1657
Fang, T., et al. 2007, ApJ, 660, L27
Fazio, G. G., et al. 2004, ApJS, 154, 10
Flores, H., et al. 1999, ApJ, 517, 148
Fomalont, E. B., et al. 1991, AJ, 102, 1258
Georgakakis, A., et al. 2007, ApJ, 660, L15
Gerke, B. F., et al. 2007, ApJ, 660, L23
Giacconi, R., et al. 2002, ApJS, 139, 369
Giavalisco, M., et al. 2004, ApJ, 600, L93
Gordon, K. D., et al. 2005, PASP, 117, 503
Hopkins, A. M., Connolly, A. J., & Szalay, A. S. 2000, AJ, 120, 2843

Huang, J.-S., et al. 2007, ApJ, 660, L69
Ivison, R., et al. 2007, ApJ, 660, L77
Kassin, S. A., et al. 2007, ApJ, 660, L35
Koekemoer, A. M., & Scoville, N. Z. 2005, NewA Rev., 49, 461
Konidaris, N., et al. 2007, ApJ, 660, L7
Le Floc'h, E., et al. 2007, ApJ, 660, L65
Lehmer, B. D., et al. 2005, ApJS, 161, 21
Lilly, S. J., Hammer, F., Le Fèvre, O., & Crampton, D. 1995, ApJ, 455, 75
Lilly, S., et al. 2005, Messenger, 121, 42
Lin, L., et al. 2007, ApJ, 660, L51
Magnier, E. A., & Cuillandre, J.-C. 2004, PASP, 116, 449
Miyaji, T., et al. 2004, AJ, 127, 3180
Moustakas, L., et al. 2007, ApJ, 660, L31
Nandra, K., et al. 2005, MNRAS, 356, 568
———. 2007, ApJ, 660, L11
Noeske, K. G., et al. 2007a, ApJ, 660, L43
———. 2007b, ApJ, 660, L47
Pierce, C. M., et al. 2007, ApJ, 660, L19
Rhodes, J., Refregier, A., & Groth, E. J. 2000, ApJ, 536, 79
Rieke, G. H., et al. 2004, ApJS, 154, 25
Rix, H.-W., et al. 2004, ApJS, 152, 163
Sarajedini, V., et al. 2006, ApJS, 166, 69
Simard, L., et al. 2002, ApJS, 142, 1
Sirianni, M., et al. 2005, PASP, 117, 1049
Steidel, C. C., Adelberger, K. L., Shapley, A. E., Pettini, M., Dickinson, M., & Giavalisco, M. 2003, ApJ, 592, 728
Stetson, P. B. 1987, PASP, 99, 191
Symeonidis, M., et al. 2007, ApJ, 660, L73
Vogt, N. P., et al. 2005, ApJS, 159, 41
Weiner, B. J., et al. 2005, ApJ, 620, 595
———. 2007, ApJ, 660, L39
Willner, S. P., et al. 2006, AJ, 132, 2159
Wilson, G., et al. 2007, ApJ, 660, L59
York, D. G., et al. 2000, AJ, 120, 1579